COBEM 2023 27TH INTERNATIONAL CONGRESS OF MECHANICAL ENGENEERING

ABCM Brazilian Society of Mechanical Sciences and Engineering
27th ABCM International Congress of Mechanical Engineering
December 04-08, 2023, Florianópolis-SC, Brazil

COB-2023-1333
A Computational Heat Transfer Model for Thermite Reaction in Offshore Well Plugging and Abandonment Operation

Rodrigo Gustavo Dourado da Silva
Thiago Dias dos Santos
Elisan dos Santos Magalhães
Instituto Tecnológico de Aeronáutica - ITA, Divisão de Pós-Graduação e Pesquisa, Praça Mal. Eduardo Gomes, 50, - Vila das Acácias, 12228-900, São José dos Campos, SP, Brazil.
rodrigodourado@ita.br, thiagotds@ita.br, elisan@ita.br

Abstract. *In the oil and gas industry, one of the most critical stages of offshore platform decommissioning is the wellbore plugging and abandonment (P&A) operation. Decommissioning standards require that, at the end of its lifespan, the wellbore be permanently sealed in order to prevent the leakage of contaminating fluids into marine ecosystems. The current decommissioning operation comprises removing the production tubing, machining the borehole casing, and cementing the machined section to seal the wellbore. Such an operation has a relatively high cost and several risks. Furthermore, the cementation does not guarantee permanent sealing due to microcracks that may appear in the cement body in the long term. An alternative technology for P&A operations is replacing cement with a metallic plug created by the thermite reaction. A thermite reaction can melt the wellbore elements, enabling the production tubing to be removed faster and creating an impermeable metallic barrier, reducing, consequently, the time and costs of P&A operations. While promising, this technology still needs further improvements to be successfully employed in real offshore oil fields. In this sense, numerical simulation is a useful tool to understand the temperature evolution inside the wellbore, optimize the parameters of the engineering problem, and design physical experiments. In this work, a two-dimensional axisymmetric finite element heat conduction model is proposed to simulate the thermite reaction inside a wellbore. The phase change of both thermite and wellbore components is calculated using the apparent heat capacity method. Also, a level set method is proposed to capture the phase change fronts and changes in thermite volume during the reaction process. The numerical results are presented and discussed.*

Keywords: *heat transfer, plugging & abandonment, thermite reaction.*

1. INTRODUCTION

Offshore oil and gas platforms are made up of modules that can be used for drilling, extraction, processing, or even temporary storage, among other tasks. Typically, a platform lasts between 30 and 40 years, or until the operating costs outweigh the revenue from the extraction of hydrocarbons. The platform is then decommissioned at this point, and the well is sealed and abandoned (Tan *et al.*, 2021). One of the most critical stages in the decommissioning of offshore platforms is the plugging and abandonment (P&A) procedure for the well. It is known that oil extraction operations result in the release of chemicals on the seabed (Mestre *et al.*, 2014). In addition, abandoned wells can serve as pathways for gas or oil to contaminate the marine environment (Abdelal *et al.*, 2015). Thus, there is a need to establish well abandonment methodologies that avoid environmental impacts while reducing the costs of the decommissioning process. Environmental requirements dictate that at the end of their lifespan, oil and gas wells must be permanently sealed to prevent the leakage of underground fluids. However, this procedure presents a high cost and no financial return for oil companies. As a comparison criterion, many offshore wells will be abandoned in the North Sea and the Gulf of Mexico in the coming years, and an estimated £3 billion will be spent on decommissioning old oil wellbores, with 50% of this value dedicated exclusively to P&A operations (Vrålstad *et al.*, 2019).

The most conventional and economical P&A operating process involves manufacturing cement plugs, which act as barriers in different well sections to prevent the leakage of oil and gas. However, microfissures may form inside the cement, which may open pathways for leaking through the plug. Additionally, micro-annuli at the cement/casing steel interface may develop due to the cement shrinkage, causing the leak (Kiran *et al.*, 2017). Leakage failures in cement-plugged wellbore are reported as the cause of serious contamination of water sources and a fatal accident in Pennsylvania in 2009 (Abdelal *et al.*, 2015). These environmental and economic concerns require alternative and innovative technologies for the P&A processes. Thermite has been widely considered as an alternate approach for wellbore closure in recent years. Thermite is a mixture of metal powder and metal oxide compound that, when activated, performs an exothermic

oxidation-reduction reaction that releases a large amount of energy. Thermite reactions can reach temperatures up to 2500 ^{o}C (Khalifeh and Saasen, 2020). One of the most common mixtures used is a combination of iron oxide and aluminum, whose stoichiometry equation is:

$$2\mathrm{Al} + \mathrm{Fe_2O_3} \longrightarrow 2\mathrm{Fe} + \mathrm{Al_2O_3} + \Delta\mathrm{H}, \tag{1}$$

where ΔH is the amount of energy generated by the reduction reaction. The idea behind the use of thermite for P&A operations is to generate enough energy through the reaction to melt the wellbore elements and the surrounding rock formation (Mortensen, 2016). This is expected to create an impermeable barrier after the materials solidify. Alternatively, the well sealing process could be performed with thermite and bismuth (Abdelal *et al.*, 2015). In this case, the thermite is used as a "heat source" to melt a bismuth volume without damaging the well components. Bismuth has two interesting properties for this application: the first is its low melting point ($\sim$271 ^{o}C), requiring a small amount of energy to reach the liquid state; the second is the fact that, unlike other metals, it expands during solidification. As a result, the bismuth plug generates pressure on the wellbore wall, and potentially penetrating the rock fissures and improving the sealing condition.

Regardless of the wellbore sealing technique using thermite, a heat transfer study should be carried out to simulate the thermal behavior in the wellbore section to be sealed. This way, it is possible to predict the temperature field over time in the various layers of the wellbore materials and verify whether the heat provided by the thermite will melt the desired wellbore components or the bismuth volume in the thermite-bismuth technology. Despite its potential application, there are few works dedicated to thermal simulations of P&A using thermite. For instance, Abdelal *et al.* (2015) developed a numerical model using the finite element method to estimate the wellbore strength during the bismuth expansion and analyzed whether the resulting wellbore sealing would resist a typical operational pressure after decommissioning; Magalhães and de Lemos (2020) estimated the temperature field evolution in a P&A using a three-dimensional finite-difference thermal model of the thermite reaction; and Zhang *et al.* (2022) used the experimental temperatures obtained by Abdelal *et al.* (2015) to estimate the heat flux acting on the inner surface of the cylindrical cavity of a sandstone specimen. In all these works, changes in the thermite domain and the evolution of the reaction front are not considered in the numerical models, which may ultimately lead to discrepancies in the estimated temperature distribution.

In this context, we develop a two-dimensional axisymmetric finite-element heat transfer model to simulate the thermite reaction propagation inside a vertical wellbore and the resulting temperature field along the steel tube. Based on a physical experiment we performed, our model considers the reaction front as a wave that propagates along the tube axis. The observed reduction in the thermite volume is also accounted in our model. We compare the calculated temperature evolution with the experimental data.

2. EXPERIMENTAL PROCEDURE

A physical experiment was conducted with the purpose of comparing experimental and modeled temperatures along the outer surface of a vertical tube. In order to evaluate the repeatability of our experimental setup, we performed three iterations of the same procedure. Figures 1a and 1b depict a three-dimensional representation of the experimental setup and the positions of five K-type thermocouples along the external surface of the tube. The experimental setup consists of an AISI 1020 steel tube with a height of 945 mm, an outer diameter of 120 mm, and an inner diameter of 75 mm. The tube was placed on an AISI 1020 base to ensure stability, and the assembly was covered with a metal protection. The purpose of the metal protection is to prevent wind influence on the temperature measurements and to avoid any damage to the thermocouples due to potentially harmful material expelled from the tube. The thermocouples were positioned with a spacing of 90 mm along the outer tube surface and fixed using capacitive discharge welding, which prevents unwanted fluctuations during the temperature acquisition.

The tube was filled with approximately 2.5 kg of thermite composed of 25% Al and 75% $\mathrm{Fe_2O_3}$ by mass, up to a height of 450 mm. During the filling process, the thermite powder was compacted to minimize its porosity. The ignition of the thermite was performed remotely using an electric initiator equipped with a pyrotechnic charge. All three experiments were performed with the same setup. The temperature was measured with a time interval of 0.5 s using a National Instruments data acquisition system NI cDaq-9189 combined with the thermocouple module NI-9213.

3. THERMAL MODEL

The transient heat diffusion equation is:

$$\rho c_p \left(\frac{\partial T}{\partial t} + \mathbf{u} \cdot \nabla T \right) = \nabla \cdot (k \nabla T) + \dot{Q}, \tag{2}$$

where T is the temperature, $\mathbf{u}$ is the fluid velocity, ρ is the density, c_p is the specific heat capacity, k is the thermal conductivity, and $\dot{Q}$ is the heat source. Here, we assume no advection effects; therefore, we set $\mathbf{u} = \mathbf{0}$. The thermal properties vary according to the thermite state (solid or fluid). We use a function $\theta = \theta\,(T) \in [0,\, 1]$ to indicate changes

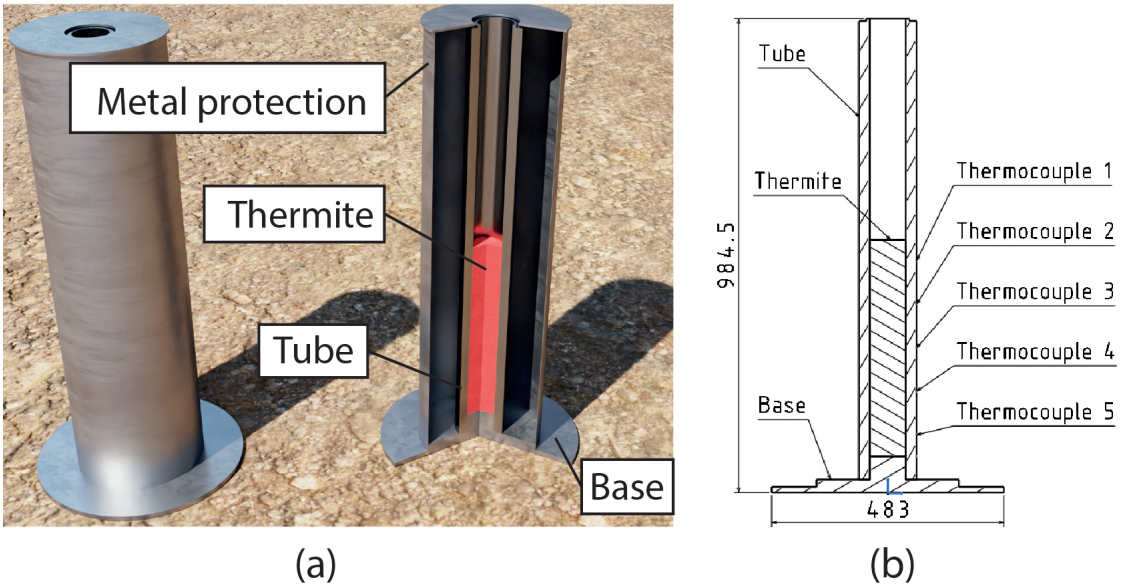

Figure 1. (a) Three-dimensional representation of the experimental setup. (b) Longitudinal section cut and thermocouple positioning (dimensions in millimeters).

in the thermal properties of the thermite:

$$\begin{aligned} \rho &= (1-\theta)\rho_s + \theta\rho_l, \\ k &= (1-\theta)k_s + \theta k_l, \\ h &= \frac{1}{\rho}\left[(1-\theta)\,\rho_s h_s + \theta\rho_f h_l\right], \end{aligned} \tag{3}$$

where h is the specific enthalpy, and subscripts s and l indicate solid and liquid states, respectively. The indicator θ is a function of the temperature, T, and it is given by:

$$\theta\left(T\right) = \begin{cases} 0, & \text{if } T \leq T_s, \\ 1, & \text{if } T \geq T_l, \\ 0.5 + 0.9375\left(2\dfrac{T-T_m}{\Delta T}\right) - 0.625\left(2\dfrac{T-T_m}{\Delta T}\right)^3 + 0.1875\left(2\dfrac{T-T_m}{\Delta T}\right)^5, & \text{if } T_s < T < T_l, \end{cases} \tag{4}$$

where T_s is the temperature at which the thermite starts to change its phase, T_l is the temperature where the thermite is totally in the fluid state, and T_m is the phase change temperature defined as:

$$T_m = \frac{T_s + T_l}{2}, \tag{5}$$

and ΔT is the temperature interval where both solid and liquid states coexist and is given by:

$$\Delta T = T_l - T_s. \tag{6}$$

In Eq. (4), the third term is the expansion of the Heaviside function centered at T_m which presents a continuous second derivative. The definition of a smooth function to indicate the phase changes as given by Eq. (4) is important for the numerical implementation of the thermite reaction developed here.

The specific heat capacity, given by the derivative of the enthalpy with respect to the temperature, i.e., $c_p = \partial h/\partial T$, is obtained with Eq. (3):

$$c_p = \frac{1}{\rho}\left[(1-\theta)\,\rho_s c_{p,s} + \theta\rho_l c_{p,l}\right] + \left(h_l - h_s\right)\frac{\partial f}{\partial T}, \tag{7}$$

where f is the mass fraction given by:

$$f = \frac{1}{2}\frac{\theta\rho_l - (1-\theta)\,\rho_s}{\rho}. \tag{8}$$

Note that, in Eq.(7), the enthalpy difference, $h_f - h_s$, is the latent heat of fusion, i.e., $(h_f - h_s) = L$. Note also that $f = -1/2$ for $T = T_s$ and $f = 1/2$ for $T = T_l$.

The heat source, $\dot{Q}$, is modeled as a thin strip (wave) of heat emission resulting from the thermite reaction front. Since the reaction develops within a finite time interval (few seconds in our experiments; see Sect. 2), we consider the heat source $\dot{Q}$ as a space- and time-dependent function, $\dot{Q} = \dot{Q}(\mathbf{x}, t)$. Although the evolution of the thermite reaction could be predicted by chemical kinetics (e.g., de Souza *et al.*, 2022; Pena and de Lemos, 2023; De Souza and de Lemos, 2023), here we consider that the reaction propagates with a velocity $\mathbf{v}_r$, which we assume to be time-dependent. We use the experimental results to adjust the velocity function (Sect. 2). We model the heat source as a continuous uniform distribution function centered at the reaction position, $\mathbf{x}_r(t)$, with a width equal to ϵ and a heat peak of $\dot{Q}_{\max}$.

We solve Eq.(2) using the finite-element method using the COMSOL Multiphysics® software (COMSOL, 2023). We employ the standard Continuous Galerkin method to describe the temperature field with a continuous piecewise function (a polynomial order equal to 2 was chosen to improve the numerical results). Due to the symmetry of our model domain (see Sect. 2and Fig. 1), and in order to save computation resources, the heat equation Eq.(2) is solved in an axisymmetric computational domain. The mesh is generated within COMSOL, and it is fixed in time. In a previous model, we used a moving mesh scheme to capture the free surface of the thermite (thermite-air interface; see Fig. 1), which moves along the time due to the decrease in the thermite volume after reaction. However, such a moving mesh approach introduced numerical inconsistency and additional computational costs. Therefore, we decide to keep the mesh fixed and employ a level-set function $\phi \in [0, 1]$ to model the thermite-air interface. In such a scheme, the thermal properties in Eq.(2) are defined as:

$$\begin{aligned} \rho &= (1-\phi)\rho_{\text{thermite}} + \phi\rho_{\text{air}}, \\ k &= (1-\phi)k_{\text{thermite}} + \phi k_{\text{air}}, \\ c_p &= (1-\phi)c_{p,\text{thermite}} + \phi c_{p,\text{air}}, \end{aligned} \tag{9}$$

where the thermite properties, ρ_{thermite}, k_{thermite}, and $c_{p,\text{thermite}}$, are functions of the thermite states as given by Eq. (3) and Eq. (7). The position of the free surface varies with time and is obtained by considering the change in the thermite volume with reaction. Also, in our model, the reaction position, $\mathbf{x}_r(t)$ is explicitly defined in the COMSOL after an analytical integral of the kinematic equation of motion with $\mathbf{v}_r$.

4. RESULTS

4.1 Experimental temperature

The temperatures obtained from the three experiments (labeled as A, B, and C) are shown in Fig. 2. The behavior of the temperature curves for the five sensors is similar in both shape and magnitude, indicating good repeatability of the experimental setup, as expected. The noise observed in the temperature of experiment A is due to the carbonization of the tape used to protect the thermocouples from external effects. In experiments B and C, this tape was replaced with a polyamide tape.

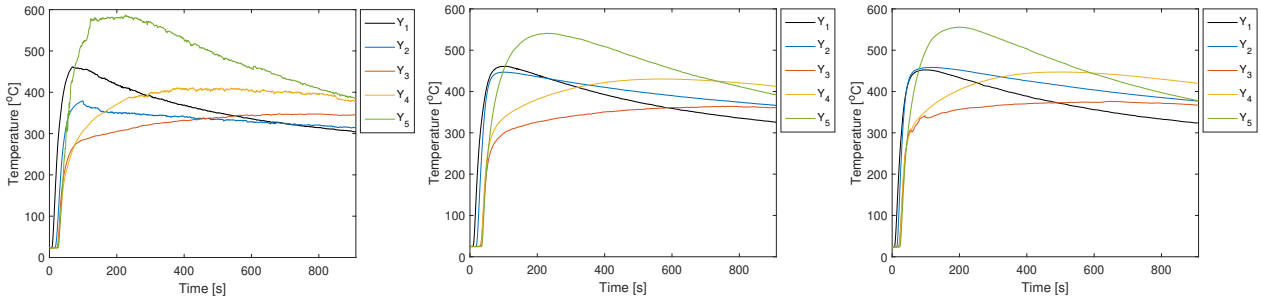

Figure 2. Experimental temperatures of experiments (a) A, (b) B and (c) C.

The highest temperature variation is observed in thermocouple Y_5 (Fig. 2), which is positioned at the bottom of the tube. This is explained by the observed heated metal plug that continues to emit a heat flux at the tube bottom after the reaction has ended. This plug has an average height of ∼92 mm, which is approximately the position of thermocouple Y_5. Figure 3 shows a longitudinal section of the tube after the experiment. In the figure, we observe two different layers of the plug, named here as a metal plug and a ceramic plug. The metal plug has a height ranging from 30 to 35 mm and is predominantly composed of iron, concentrated at the bottom due to its high density. The upper layer of the plug, the ceramic plug, is composed of a ceramic material, predominantly consisting of aluminum oxide, which is also present as a thin layer of approximately 3 mm adhered to the inner surface of the tube due to fast solidification.

Figure 3. (a) Longitudinal section of the tube after the experiment and the thermite reaction products: a metal plug, a ceramic plug, and a ceramic layer along the inner surface. (b) Detailed view of the final plug (metal and ceramic plugs).

The temperature sensors located in the intermediate sections, Y_3 and Y_4, showed the smallest and slowest temperature variations. This can be explained by the rapid decrease in thermite volume during the reaction process. As a result, the tube sections where such thermocouples are positioned do not remain in contact with the molten thermite products for a long time, and a large portion of the energy received in those regions is due to heat diffusion along the tube.

The response time of the temperature for each thermocouple is shown in Fig. 4. The response time identifies the delay in temperature variation relative to the beginning of the reaction. The curves in Fig. 4 exhibit a non-linear behavior, suggesting that the reaction front propagates with a variable velocity along the vertical tube.

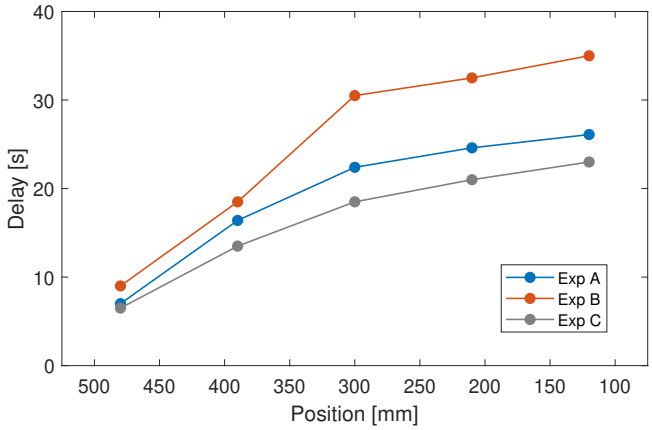

Figure 4. Response time of temperature relative to the beginning of the reaction as a function of thermocouple positions. The three experiments are shown.

4.2 Thermal model temperature

After the physical experiments, we run several numerical experiments to validate the developed thermal model described in Sect. 3. We assume that the thickness of the reaction front is constant and equal to 2 mm, and the internal energy generation during the reaction is 9×10^{10} W/m^3. The average reaction velocity as a function of time was estimated based on the temperature response of experiment C.

The model temperatures at the thermocouple positions are shown in Fig. 5. The experimental temperatures for experiment C are also shown in that figure. We show the results of three different model configurations: a) constant thermite volume; b) decrease in thermite volume with constant reaction velocity; and c) decrease in thermite volume with time-dependent reaction velocity.

As seen in Fig. 5a, considering a constant thermite volume, the temperatures at the intermediate tube positions (T_2, T_3, and T_4) exceed the temperatures at position T_5, which does not correspond to the experimental result. Modeling a decrease in thermite volume and assuming a constant reaction velocity (Fig. 5b), the highest temperature variation is obtained at sensor T_5 due to the accumulated thermite mass at the bottom of the vertical tube. However, the temperature variation at the positions of the sensors T_1, T_2, and T_3 is much lower than the temperatures obtained experimentally. With

both volume reduction and variable reaction velocity, the model generates temperature profiles closer to the experimental data (Fig. 5c).

The evolution of the liquid fraction (Θ) in the thermite domain during the reaction for model C (i.e., the model considering both the decrease in thermite volume and the time-dependent reaction velocity) is illustrated in Fig. 6. Note the reduction in thermite volume from $t = 0$ to $t = 31$ s, which is the end of the reaction. Following the completion of the thermite reaction, the melted mass at the bottom of the tube initiates the solidification process, as depicted in Fig. 6 at $t = 50$ s. The resulting solidified plug in the simulation is 91 mm high, which is very consistent with the experimental results.

Table 4.2 shows the maximum temperature, T_{max}, at each temperature sensor for the three experiments and numerical model C. The measurement uncertainty, according to Holman (2012), for the K-type thermocouple (chromel-alumel) is 0.75% and is also shown in the table. The values of T_{max_1}, T_{max_2}, and T_{max_5} calculated by the numerical model C fall within the experimental data range. However, T_{max_3} and T_{max_4} showed lower values than the experimental ones. This can be explained by variations in the reaction thickness during the reaction, and further experiments should be conducted to investigate the model's sensitivity to such physical parameters.

Table 1. Maximum temperature at each sensor in experiments A, B, and C and in the numerical model.

	T_{max_1}	T_{max_2}	T_{max_3}	T_{max_4}	T_{max_5}
Exp A	461,6 ± 3,5	379,3± 2,8	347,8 ± 2,6	411,0 ± 3,1	587,6 ± 4,4
Exp B	461,1 ± 3,5	446,9 ± 3,4	364,4 ± 2,7	430,5 ± 3,2	541,1 ± 4,1
Exp C	452,4 ± 3,4	458,3 ± 3,4	376,2 ± 2,8	447,2 ± 3,4	555,7 ± 4,2
Model	453.7	438.2	306.8	397.3	569.7

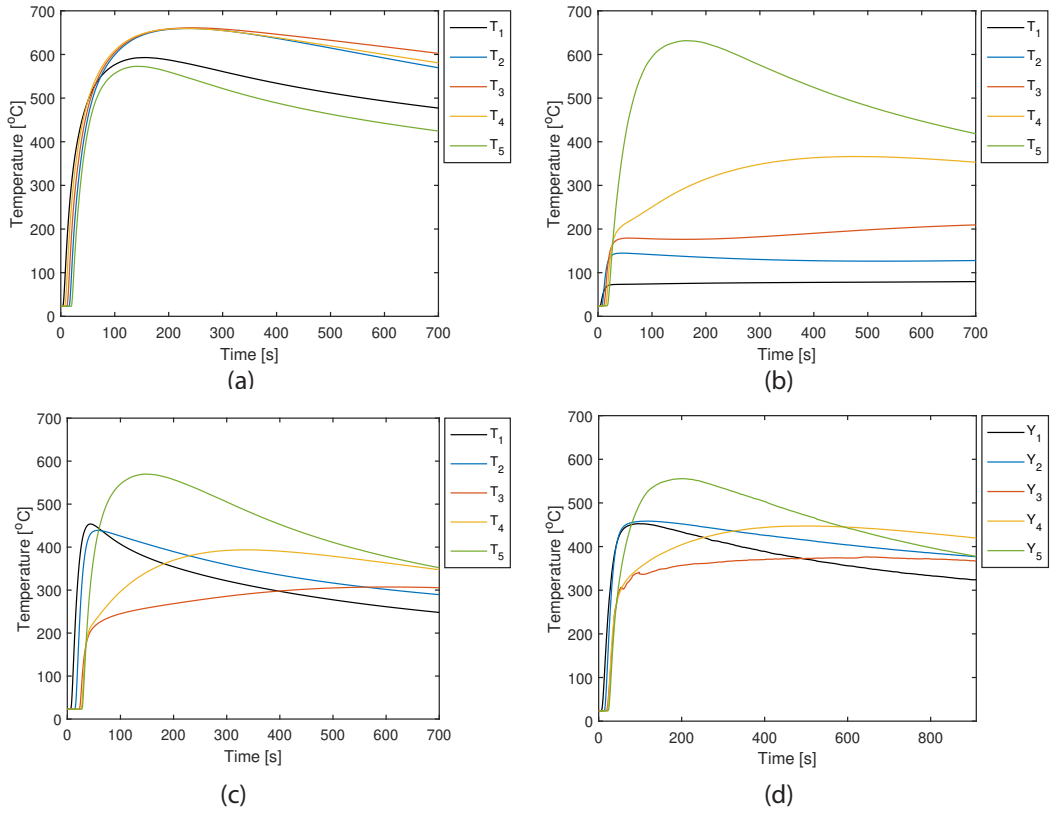

Figure 5. Model (T) and experimental temperatures (Y). (a) Model without considering the reduction in the thermite volume. (b) Model with a decrease in thermite volume and constant reaction velocity. (c) Model with a decrease in thermite volume and time-dependent reaction velocity. (d) Experimental temperatures.

5. CONCLUSIONS

A two-dimensional, axisymmetric finite-element thermal model was developed to simulate the thermite reaction inside a wellbore. Such a model evaluates the temperature field, the phase change, and the liquid fraction of the components

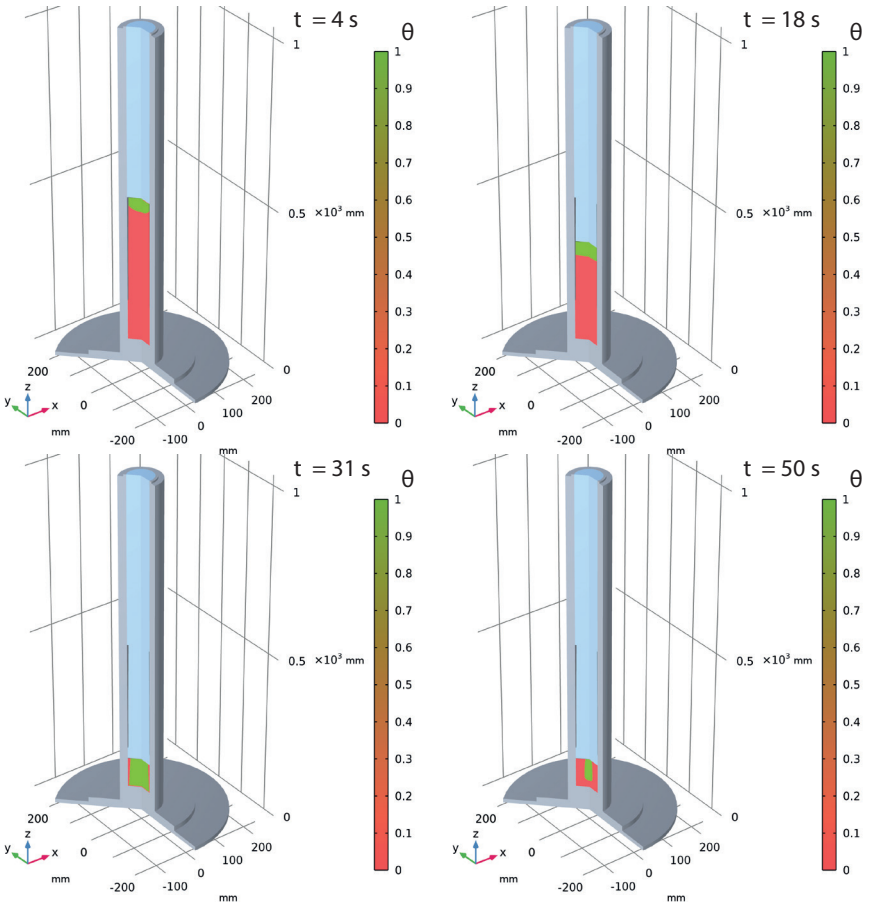

Figure 6. Liquid fraction (θ) and volume reduction along the simulation time.

of a wellbore using the heat capacity model. By comparing the temperatures from a physical experiment, we found that a time-dependent reaction velocity ($\mathbf{v}_r(t)$) better explains the observed data. In future work, we will estimate the critical parameters of the model during the thermite reaction using advanced inverse problem techniques. The model developed here has the potential to be used as a design tool for plugging and abandonment operations with thermite and bismuth-based technologies.

6. ACKNOWLEDGEMENTS

The authors would like to thank the brazilian sponsors PETROBRAS and CNPq for their financial support.

7. REFERENCES

Abdelal, G.F., Robotham, A. and Carragher, P., 2015. "Numerical simulation of a patent technology for sealing of deep-sea oil wells using nonlinear finite element method". *Journal of Petroleum Science and Engineering*, Vol. 133, pp. 192–200. ISSN 0920-4105. doi:https://doi.org/10.1016/j.petrol.2015.05.010. URL `https://www.sciencedirect.com/science/article/pii/S0920410515002016`.

COMSOL, 2023. COMSOL Multiphysics® v. 6.1, www.comsol.com, COMSOL AB, Stockholm, Sweden.

de Souza, K.M., de Lemos, M.J.S. and Kawachi, E.Y., 2022. "Thermodynamics of thermite reactions for a new thermal plug and abandonment process". *Continuum Mechanics and Thermodynamics*, Vol. 34, No. 1, pp. 259–271. ISSN 1432-0959. doi:10.1007/s00161-021-01056-6. URL `https://doi.org/10.1007/s00161-021-01056-6`.

De Souza, K.M. and de Lemos, M.J., 2023. "Advanced one-dimensional modeling of thermite reaction for thermal plug and abandonment of oil wells". *International Journal of Heat and Mass Transfer*, Vol. 205, p. 123913. ISSN 0017-9310. doi:https://doi.org/10.1016/j.ijheatmasstransfer.2023.123913. URL `https://www.sciencedirect.com/science/article/pii/S0017931023000686`.

Holman, J., 2012. *Experimental Methods for Engineers*. Economia e discipline aziendali. McGraw-Hill/Connect Learn Succeed. ISBN 9780071326483.

Khalifeh, M. and Saasen, A., 2020. *Introduction to Permanent Plug and Abandonment of Wells*. Springer, Cham.

Kiran, R., Teodoriu, C., Dadmohammadi, Y., Nygaard, R., Wood, D., Mokhtari, M. and Salehi, S., 2017. "Identification

and evaluation of well integrity and causes of failure of well integrity barriers (a review)". *Journal of Natural Gas Science and Engineering*, Vol. 45, pp. 511–526. ISSN 1875-5100.

Magalhães, E. and de Lemos, M.J., 2020. "A thermal study of a new oil well plugging & abandonment operation". *International Journal of Thermal Sciences*, Vol. 155, p. 106421. ISSN 1290-0729.

Mestre, N.C., Calado, R. and Soares, A.M., 2014. "Exploitation of deep-sea resources: The urgent need to understand the role of high pressure in the toxicity of chemical pollutants to deep-sea organisms". *Environmental Pollution*, Vol. 185, pp. 369–371. ISSN 0269-7491.

Mortensen, F.M., 2016. *A New P&A technology for setting the permanent barriers*. Ph.D. thesis, University of Stavanger.

Pena, F.J. and de Lemos, M.J., 2023. "Simulation of multidimensional unsteady heat transfer with aluminothermic reaction and phase transition". *International Journal of Heat and Mass Transfer*, Vol. 213, p. 124365. ISSN 0017-9310. doi:https://doi.org/10.1016/j.ijheatmasstransfer.2023.124365. URL `https://www.sciencedirect.com/science/article/pii/S0017931023005112`.

Tan, Y., Li, H.X., Cheng, J.C., Wang, J., Jiang, B., Song, Y. and Wang, X., 2021. "Cost and environmental impact estimation methodology and potential impact factors in offshore oil and gas platform decommissioning: A review". *Environmental Impact Assessment Review*, Vol. 87, p. 106536. ISSN 0195-9255.

Vrålstad, T., Saasen, A., Fjær, E., Øia, T., Ytrehus, J.D. and Khalifeh, M., 2019. "Plug & abandonment of offshore wells: Ensuring long-term well integrity and cost-efficiency". *Journal of Petroleum Science and Engineering*, Vol. 173, pp. 478–491. ISSN 0920-4105.

Zhang, J., Sun, R., Li, Z., Li, X., Tao, H., Wang, Z., Yu, S. and Zhang, W., 2022. "Control Model and Optimization Study of Temperature Distribution Applied in Thermite Plugging and Abandonment Technology". *Journal of Energy Resources Technology*, Vol. 145, No. 3.

8. RESPONSIBILITY NOTICE

The authors are solely responsible for the printed material included in this paper.